Electronic Supplementary Information (ESI)

Quantifying the Optimal Thickness in Polymer:Fullerene Solar Cells from the Analysis of Charge Transport Dynamics and Photoabsorption

Shaoxian Li,[a] Fumiya Hamada,[a] Ryosuke Nishikubo,[a] and Akinori Saeki[*, a, b]*

[a]Department of Applied Chemistry, Graduate School of Engineering, Osaka University, 2-1 Yamadaoka, Suita, Osaka 565-0871, Japan.

[b]Innovative Catalysis Science Division, Institute for Open and Transdisciplinary Research Initiatives (ICS-OTRI), Osaka University, 1-1 Yamadaoka, Suita, Osaka 565-0871, Japan.

AUTHOR INFORMATION

Corresponding Author

*saeki@chem.eng.osaka-u.ac.jp (A.S.)

This supporting information presents the following contents.

Supplementary Note S1

General principle of TOF-TRMC measurement. The key of TOF-TRMC measurement is to separate the carrier mobility from the mobility-containing signal. Δ*P* is the transient of reflected microwave power in the TRMC measurement, which is proportional to the photoconductivity Δ*σ*. Δ*σ* is related with the carrier mobility in the following equation: $\Delta\sigma = en\Sigma\mu$, where *n* is the photogenerated charge carrier density, *e* is the elementary charge, and Σ*μ* is the sum of photogenerated hole and electron mobilities. In the TOF-TRMC, holes or electrons are swept out under the applied voltage; thus, Σ*μ* is treated as *μ* (hole for HOD and electron for EOD). In order to separate *μ* from Δ*σ* measured by TRMC technique, the key is to determine the time-dependent carrier density. The carrier density is subjected to two factors: carrier recombination and electrode collection, which are analysed separately in TOF-TRMC measurement. In our strategy, this time-dependent carrier density is calculated using a combination of TOF-TRMC measurement and bulk-recombination simulation. The calculation formula is expressed by $\mu = K\Delta P\,(\Delta I\, n^{re})^{-1}$. *K* is a scaling factor mostly independent on measured samples. The Δ*I* refers to the TPC transients (obtained in simultaneous TOF measurement) of an OSC device under external electric field, which shows the charge carrier extraction by electrode. Through diving Δ*P* with Δ*I*, the proportion of charge carrier density contributed from electrode extraction can be calibrated, although this calibration is not so important. n^{re} refers to the carrier density in a response to bulk recombination of charge carriers. For n^{re} analysis, we used simulation based on one-dimensional carrier diffusion under external electric field and second-order recombination theory (shown in eqns (2) and (3)). Through diving Δ*P* with n^{re}, the proportion of charge carrier density that is contributed from charge carrier bulk recombination can be calibrated. Thus, time-dependent carrier mobility is separated, and the mobility relaxation characteristics are obtained.

Supplementary Note S2

Reasons for fitting Δ*P*/Δ*I* (norm) curve with $n^{re}(t)$ under low *E*. The TPC transients (Δ*I*) may be affected by deep traps and recombination with dark carriers; thus, the TRMC signal (Δ*P*) was normalized by Δ*I* as explained in Note S1, although the effect of this normalization is marginal. In addition, the contribution of bulk recombination and charge extraction should be removed from the TRMC decay to extract the mobility relaxation. Accordingly, the carrier density: $n^{re}(t)$ calculated from the diffusion theory was used to fit the experimental Δ*P*/Δ*I* curve (normalized) under the low electric field. For EOD, the φ_{EOP} values obtained in our analysis are 1×10^{-4}, 3.6×10^{-3}, 1.5×10^{-4} for P3HT:PCBM, PffBT4T:PCBM and PCPDTBT:PC_{71}BM. For HOD, the φ_{EOP} values obtained in our analysis are 1.4×10^{-3}, 8×10^{-4}, 9.5×10^{-5} for P3HT:PCBM, PffBT4T:PCBM and PCPDTBT:PC_{71}BM.

Supplementary Note S3

Stretched exponential function for mobility relaxation quantification. It is crucial to quantify the mobility relaxation behaviour of different BHJ samples. At first we tried fitting the mobility relaxation curve using the following double-exponential function ($A_1 + A_2 = 1$):

$$(\mu_{normalized} = A_1 \cdot e^{-k_1 t} + A_2 \cdot e^{-k_2 t})$$

, where the mobility relaxation lifetime τ^{re} was obtained as $A_1\tau_1+A_2\tau_2$. However, we found that the lifetime calculated using this function reflects mostly the mobility relaxation behaviour in the late period side (**Fig. S8b**), while our mobility relaxation analysis is more important in the early period side. In addition, the data accuracy in the late period is not good, because of the small n^{re} and large fluctuation of TRMC transient. Instead, we used the stretched exponential function (shown in eqn 5) for fitting and thus more reasonable mobility relaxation lifetime was obtained (**Fig. S8a**). The stretched exponential function is often used to fit a decay curve of photoluminescence (PL), TRMC, and transient absorption spectroscopy (TAS). It is understood as a dispersive diffusion in a media that leads to a fast decay in the short time range and slow decay in the long time range (e.g. J. Kakalios et al., *Phys. Rev. Lett.* 1987, **59**, 1037). We speculate that the mobility relaxation kinetics (β ~ 0.5, **Fig. S8a**) follows a fast and slow relaxation with the elapse of time, as a result of spatially distributed density of state (DOS).

Supplementary Note S4

Explanation on the statement that *k* possibly falls into the range of 0<*k*<3. The *k* can be written as $k = k_1/k_2$ (k_1, k_2 >0), where k_1 is the multiplier of term $L_eL_h(L_e+L_h)^{-1}$ and k_2 is the multiplier of term $\ln(\mu_e^0/\mu_h^0+\mu_h^0/\mu_e^0)$. Here we discuss them separately. The term $k_1 \cdot L_eL_h(L_e+L_h)^{-1}$ considers that in OSCs, the total (or effective) carrier diffusion length is dominant by the charge carrier with the shorter diffusion length, as pointed out in many other

literatures. Using this term, the calculated value is mainly determined by the smaller one of L_e or L_h. For example, if $L_e << L_h$, then $k_1 \cdot L_e L_h (L_e+L_h)^{-1} \approx k_1 \cdot L_e$. The most balanced diffusion length ($L_e = L_h$) leads this term to $k_1 \cdot L_e/2$ (or $k_1 \cdot L_h/2$). Also, in any conditions, $k_1 \cdot L_e L_h (L_e+L_h)^{-1}$ should not exceed (L_e+L_h). Thus, from $k_1 \cdot L_e L_h (L_e+L_h)^{-1} < L_e+L_h$ and $L_e = L_h$, we obtain $k_1 < 4$.

The term $k_2 \cdot \ln(\mu_e^0/\mu_h^0+\mu_h^0/\mu_e^0)$ calibrates the effect of space charge accumulation caused by mobility imbalance on the d_{eff}. The logarithm function is used to avoid overestimation of the role of mobility imbalance. This term becomes the minimum of $k_2 \ln 2$ at $\mu_e^0 = \mu_h^0$, while d_{eff} becomes the maximum. $k_2 \ln 2$ should not exceed the unity; and thus, $k_2 > (\ln 2)^{-1}$. By combining $k_1 < 4$ and $k_2 > (\ln 2)^{-1}$, we assume that $0 < k = k_1/k_2 < 2.77.. \approx 3$.

In addition, within this k range, the effect of k variation on L_{opt} determination can be well compensated through selecting a proper k' in eqn (9) (shown in **Fig. S8**). Thus, we conclude that $0 < k < 3$ is a reasonable range, although $k > 10$ values still allow for a good fit with the experiment by adjusting k'.

Supplementary Note S5

Complementary explanation on the free-transport region model. In this paper, we propose an imaginary free-transport region for charge carriers, after calibrating hole/electron effective diffusion length (morphology-dependent) and space-charge effect (mobility-balance-dependent). Thus, within the free-transport region, any morphological and structural information (including tail state levels) will not be further considered. Though only empirical, we consider charge carriers in this calibrated region will not be affected by any structural disorders, tail states and defects, so there will ideally be no mobility relaxation in this region, leading to a constant carrier mobility (and drift velocity). Further, because the solar cell is under continuous sunlight illumination, we consider the charge carrier generation rate in this part is also constant. Thus, the charge carriers in this imaginary region will distribute evenly, with a certain carrier density. Though the detailed value of this carrier density is not calculable due to the free-transport region being totally imaginary, we consider them to be material-independent since all the differences in material-dependent information (especially, the morphology) has been cancelled due to calibration. Therefore, the photogenerated charge carrier number (d_{eff}- and $\alpha_{AM1.5G}$-dependent) in this region is considered proportional to the L_{opt}. After calculating the photogenerated charge carrier number in this free-transport region, the k' in eqn (9) can be identified through fitting the calculated L_{opt}-E plot with the experimental L_{opt} range. After that, the L_{opt} determination formula based on the above free-transport region model is completed. This is the concept for our half-empirical L_{opt} determination model.

Supplementary Note S6

Morphology dependence of P3HT:PCBM processed from DCB or CB. In order to confirm the morphology dependence of our L_{opt} determination, we prepared the TOF-TRMC devices using the same preparation conditions as that in literature[69], either using DCB or CB solvent (the film thickness is 2.4–3.2 μm). Then we analysed the samples while using the corresponding bimolecular recombination coefficients[69] of 1×10^{-13} cm^3/s for P3HT:PCBM (DCB) and 2×10^{-12} cm^3/s for P3HT:PCBM (CB). The TOF results (**Fig. S10**) show that the electron mobility is much larger than hole mobility, and thus hole transport is more decisive in the L_{opt} determination. As listed in **Table S2**, the mobility at zero electric field was calculated to be $3.8 \times 10^{-2}/3.8 \times 10^{-3}$ $cm^2\ V^{-1}\ s^{-1}$ for electron/hole in P3HT:PCBM (DCB) and $5.7 \times 10^{-2}/3.3 \times 10^{-3}$ $cm^2\ V^{-1}\ s^{-1}$ for electron/hole in P3HT:PCBM (DCB). The electron/hole mobility ratio is 10 in P3HT:PCBM (DCB) and 17 in P3HT:PCBM (CB), showing P3HT:PCBM (DCB) has a more balanced electron/hole mobility ratio, which is beneficial for reducing the space charge effect. The mobility relaxation result (**Figs. S11 and S12**) shows that P3HT:PCBM (DCB) and P3HT:PCBM (CB) have similar electron mobility relaxation characteristics, yet the hole mobility relaxation of P3HT:PCBM (CB) is more prompt than that of P3HT:PCBM (DCB), leading to the shorter L_{di} of holes in P3HT:PCBM (CB). Also, P3HT:PCBM (DCB) shows better photoabsorption characteristics compared with that of P3HT:PCBM (CB). As a result, the calculated L_{opt} is around 180–300 nm for P3HT:PCBM (DCB), and 60–110 nm for P3HT:PCBM (CB), which is consistent with the L_{opt} reported by that literature (around 180–320 nm for P3HT:PCBM (DCB) and 65–100 nm for P3HT:PCBM (CB)). The results confirmed that our L_{opt} determination is closely related with the BHJ layer's morphology, and is effective only under the same preparation conditions (except for sample thickness).

In addressing the reason for the L_{opt} difference between P3HT:PCBM (DCB) and P3HT:PCBM (CB), as the literature[69] has pointed out, the evaporation speed of DCB is much slower than that of CB, offering the dropped P3HT:PCBM (DCB) solution enough time to grow into large crystalline size (also with better crystallinity) during solvent evaporation. In all, the better crystallinity, less tail state density and reduced recombination in P3HT:PCBM (DCB) renders it a more balanced mobility ratio, slower mobility relaxation and better photoabsorption, which are considered important factors that lead to the larger L_{opt}.

Table S1. List of electric field strength applied to the device (Fig. 2)

(panel in Fig. 2) sample	Device	L (μm)[a]	Trace No. (1: blue to 13-16: Red)															
			1	2	3	4	5	6	7	8	9	10	11	12	13	14	15	16
			E (10^4 V cm^{-1})															
(a) P3HT:PCBM	EOD	2.53	0.18	0.23	0.35	0.47	0.59	0.69	0.93	1.2	1.4	1.6	1.8	2.0	2.2	3.1	3.9	-
(b) PffBT4T:PCBM	EOD	2.34	0.34	0.38	0.43	0.64	0.85	1.1	1.3	1.7	2.1	2.6	3.0	3.4	3.8	4.3	6.4	-
(c) PCPDTBT:$PC_{71}BM$	EOD	1.95	0.57	0.66	0.76	0.85	0.95	1.4	1.9	2.4	2.8	3.8	4.7	5.7	6.6	7.6	8.5	9.5
(d) P3HT:PCBM	HOD	1.05	0.51	0.77	1.0	1.3	1.5	2.1	2.6	3.1	3.6	4.1	4.6	5.1	7.7	10	-	-
(e) PffBT4T:PCBM	HOD	2.60	0.19	0.38	0.77	1.2	1.5	1.9	2.3	2.7	3.1	3.5	3.8	5.8	7.7	-	-	-
(f) PCPDTBT:$PC_{71}BM$	HOD	2.09	0.48	0.72	0.96	1.2	1.4	1.9	2.4	2.9	3.3	3.8	4.3	4.8	7.2	9.6	-	-

[a] Thickness of the active layer.

Table S2. Summary of P3HT:PCBM processed from DCB and CB prepared by following the process in the literature.[69]

Solvent	Film thickness / μm	μ_e^0 /cm^2 V^{-1} s^{-1}	μ_h^0 /cm^2 V^{-1} s^{-1}	μ_e^0/μ_h^0	L_{opt} (model) / nm	L_{opt} (reported)[69] / nm
DCB	2.42 ±0.45 (EOD); 3.09 ±0.19 (HOD)	3.8×10^{-2}	3.8×10^{-3}	10	180–300	180–320
CB	3.15 ±0.44 (EOD); 2.84 ±0.56 (HOD)	5.7×10^{-2}	3.3×10^{-3}	17	60–110	65–100

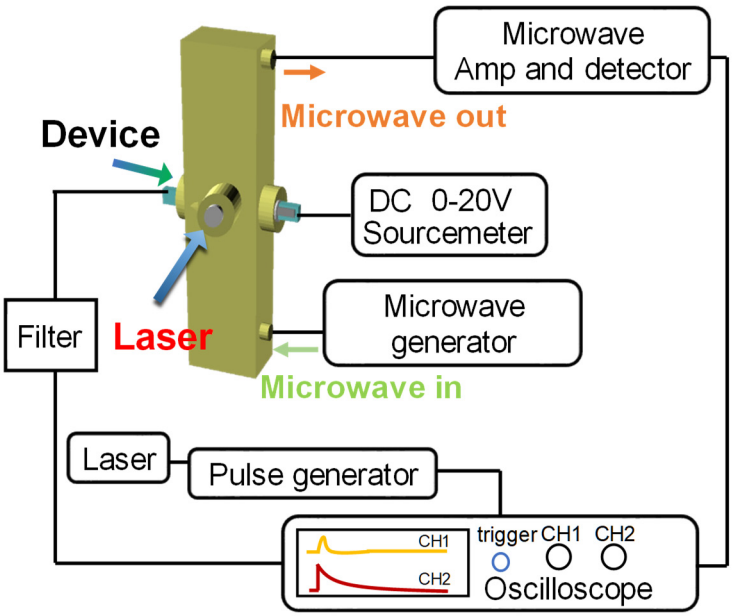

Figure S1. Schematic of the TOF-TRMC measurement system.

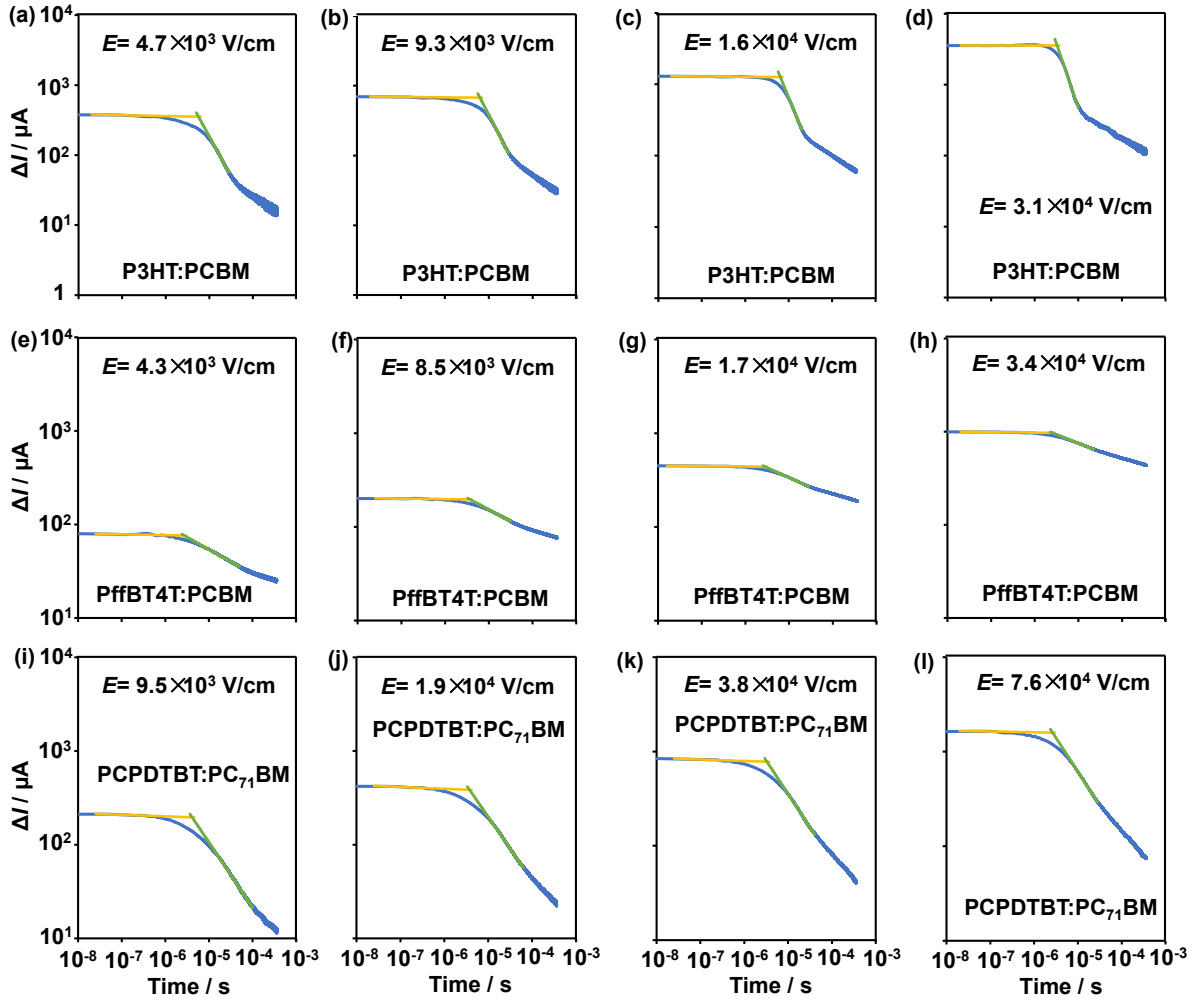

Figure S2. TPC transient analysis of EOD devices under various electric field strength (four data are picked up from totally 13-16 data, Table S1). (a-d) P3HT:PCBM, (e-h) PffBT4T:PCBM, (i-l) PCPDTBT:$PC_{71}BM$. The TOF time (τ_{TOF}) is evaluated from the intersection of the extrapolate two lines (green and yellow).

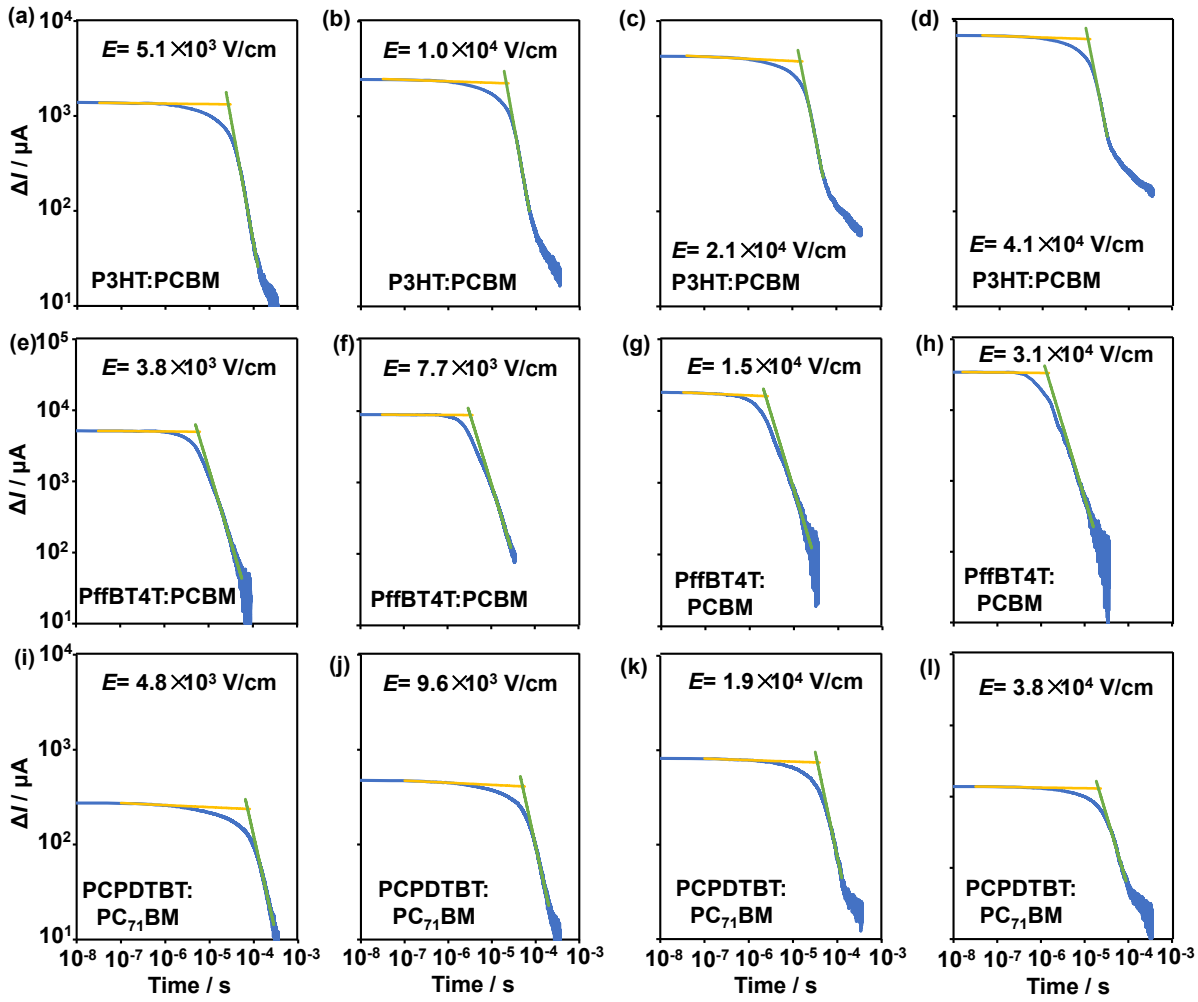

Figure S3. TPC transient analysis of HOD devices under various electric field strength (four data are picked up from totally 13-16 data, Table S1). (a-d) P3HT:PCBM, (e-h) PffBT4T:PCBM, (i-l) PCPDTBT:$PC_{71}BM$. The TOF time (τ_{TOF}) is evaluated from the intersection of the extrapolate two lines (green and yellow).

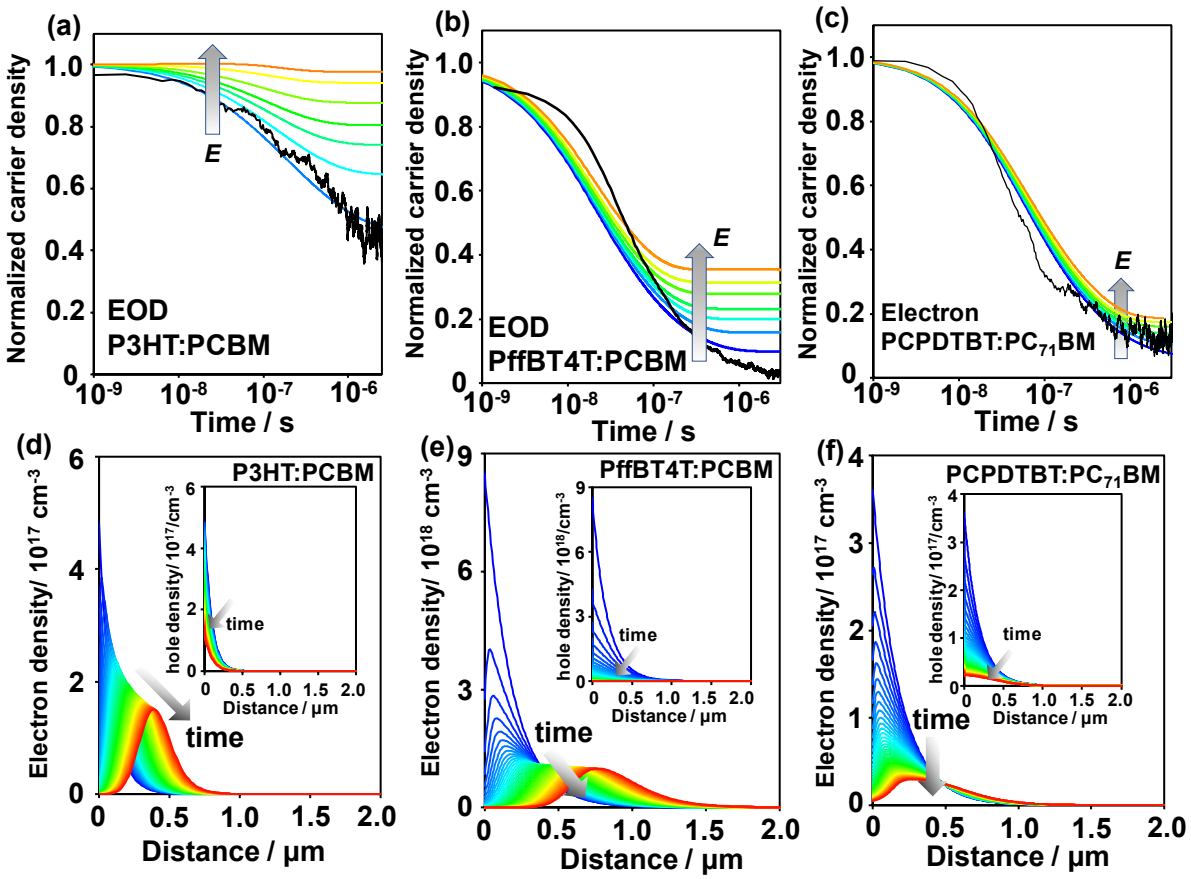

Figure S4. Normalized charge carrier probability of EOD devices in (a) P3HT:PCBM at E= (0.23–3.1) × 10^4 V cm^{-1}, (b) PffBT4T:PCBM at E= (0.43–4.3) × 10^4 V cm^{-1} and (c) PCPDTBT:PC_{71}BM at E= (0.95–8.5) × 10^4 V cm^{-1}. The time evolution of charge carrier spatial distribution (inset: hole density) of (d) P3HT:PCBM at E= 3.1×10^4 V cm^{-1}, (e) PffBT4T:PCBM at E= 4.3×10^4 V cm^{-1} and (f) PCPDTBT:PC_{71}BM at E= 8.5×10^4 V cm^{-1}.

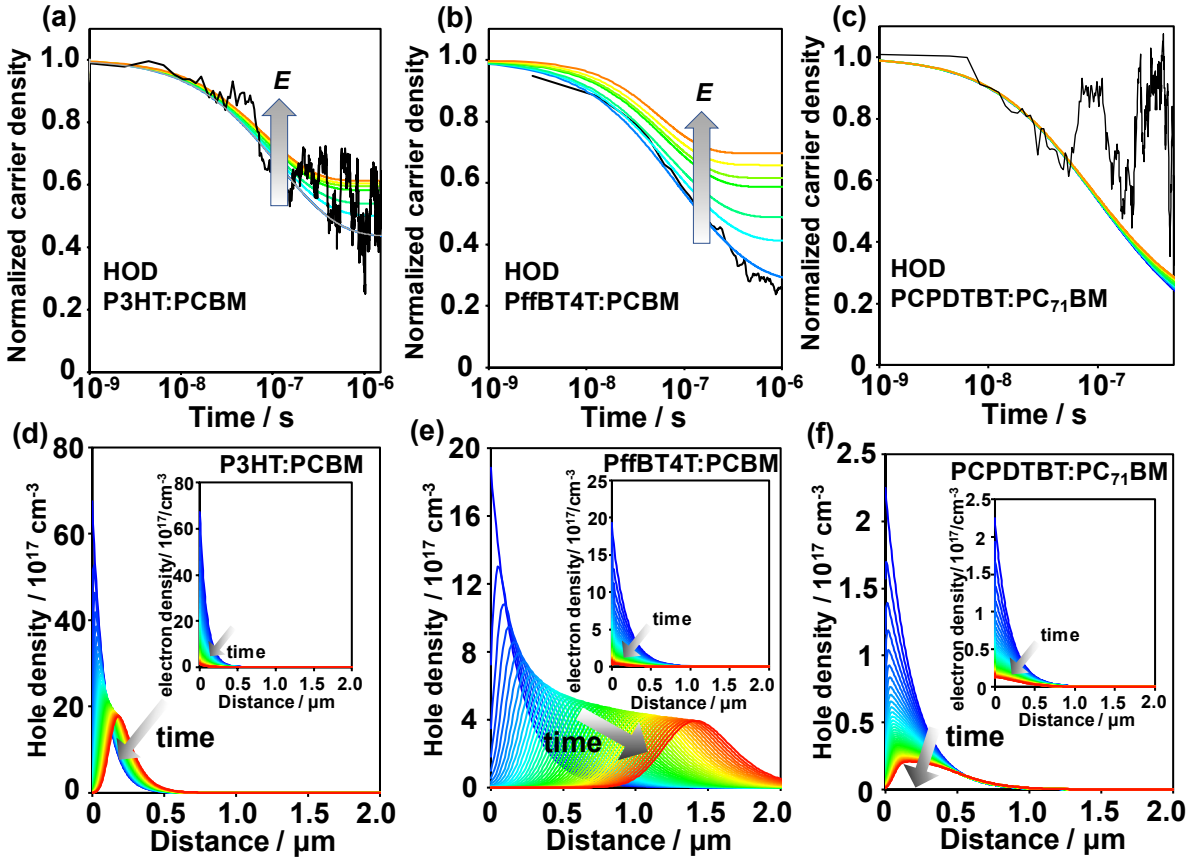

Figure S5. Normalized charge carrier probability of HOD devices in (a) P3HT:PCBM at E= (1.0–5.1) × 10^4 V cm^{-1}, (b) PffBT4T:PCBM at E= (0.38–3.8) × 10^4 V cm^{-1} and (c) PCPDTBT:PC_{71}BM at E= (0.48–4.8) × 10^4 V cm^{-1}. The time evolution of charge carrier spatial distribution (inset: electron density) of (d) P3HT:PCBM at E= 5.1×10^4 V cm^{-1}, (e) PffBT4T:PCBM at E= 3.8×10^4 V cm^{-1} and (f) PCPDTBT:PC_{71}BM at E= 4.8×10^4 V cm^{-1}.

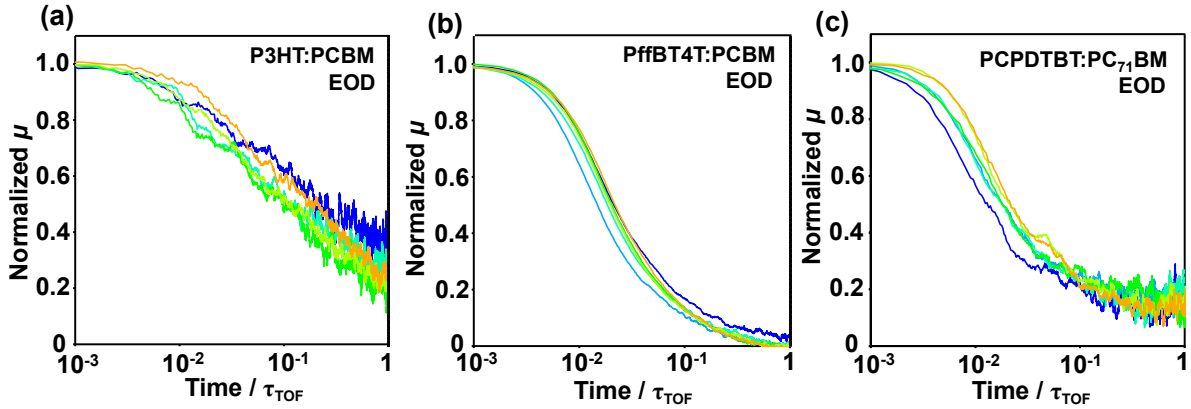

Figure S6. Normalized electron mobility as a function of time/τ_{TOF} under various E. (a) P3HT:PCBM at E= (0.23–3.1) × 10^4 V cm^{-1} (b) PffBT4T:PCBM at E= (0.43–4.3) × 10^4 V cm^{-1} and (c) PCPDTBT:PC_{71}BM at E= (0.95–8.5) × 10^4 V cm^{-1}.

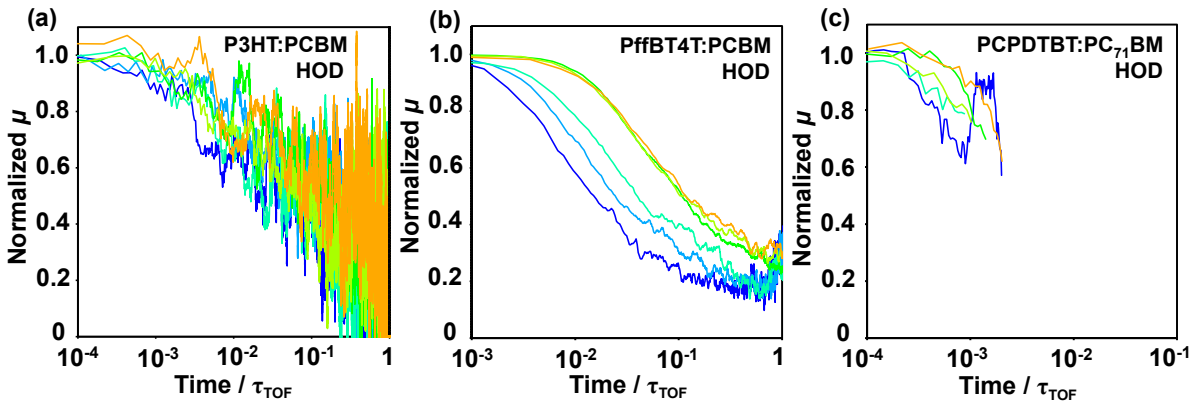

Figure S7. Normalized hole mobility as a function of time/τ_{TOF} under various E. (a) P3HT:PCBM at E= (1.0–5.1) × 10^4 V cm^{-1} (b) PffBT4T:PCBM at E= (0.38–3.8) × 10^4 V cm^{-1} and (c) PCPDTBT:$PC_{71}BM$ at E= (0.48–4.8) × 10^4 V cm^{-1} (time/τ_{TOF} > 0.002 is not shown due to large noise from baseline).

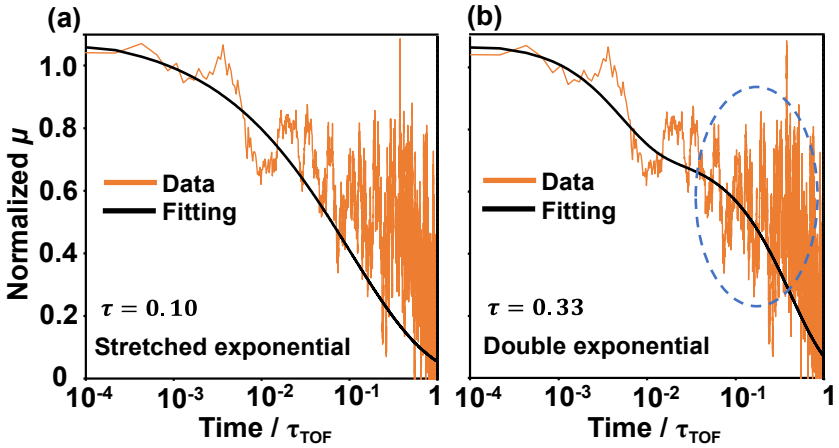

Figure S8. Comparison of fitting the same mobility relaxation profile using (a) stretched exponential function and (b) double exponential function. The calculated τ (time/τ_{TOF}) based on the fitting result is appended in the bottom left of each graph. The blue dash ellipse in (b) shows the fluctuation of baseline in the late period, which results in a significant overestimation of the calculated τ in double exponential function. Sample: P3HT:PCBM HOD at E= 5.1×10^4 V cm^{-1}.

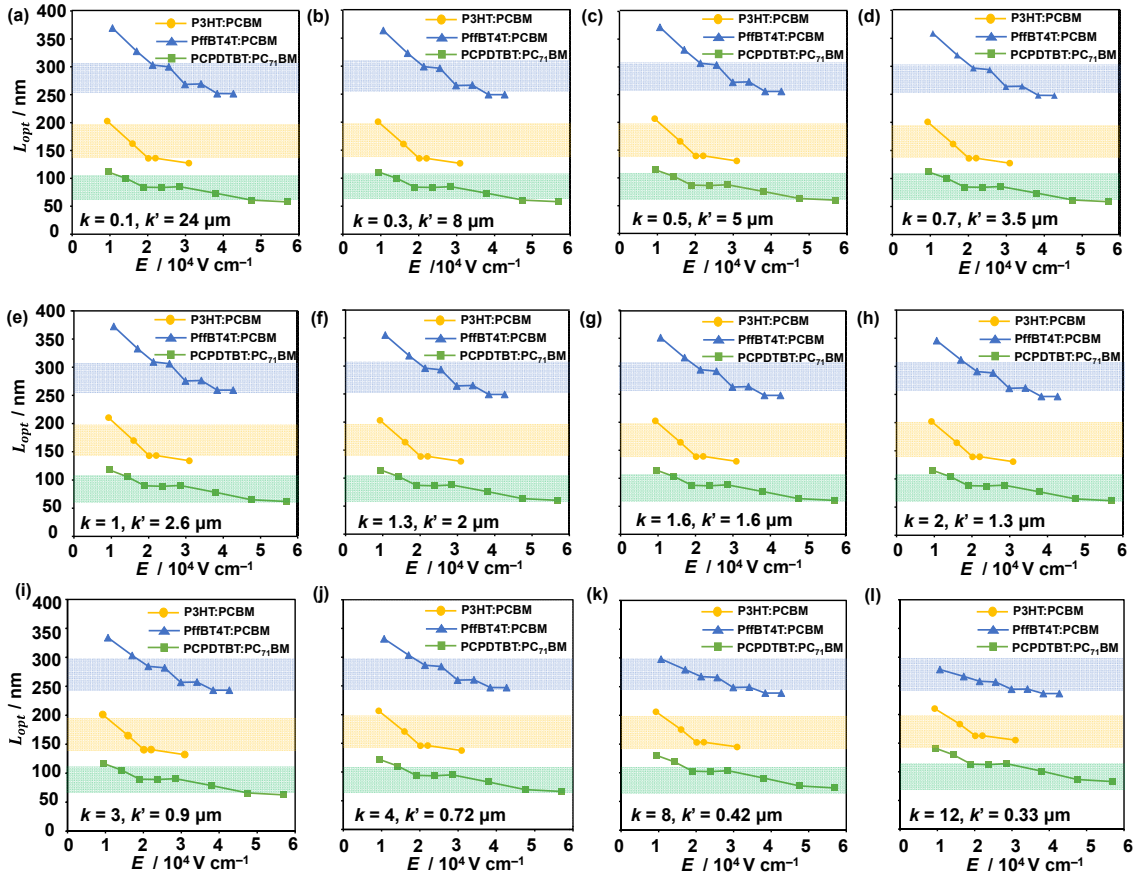

Figure S9. (a-l) Calculated L_{opt} as a function of electric field using a different set of k and k' values. Width of the correspondently coloured ribbon shows the reported L_{opt} range from experimental data. A good correspondence between the experimental and calculated L_{opt} are obtained by a different set of k and k' values.

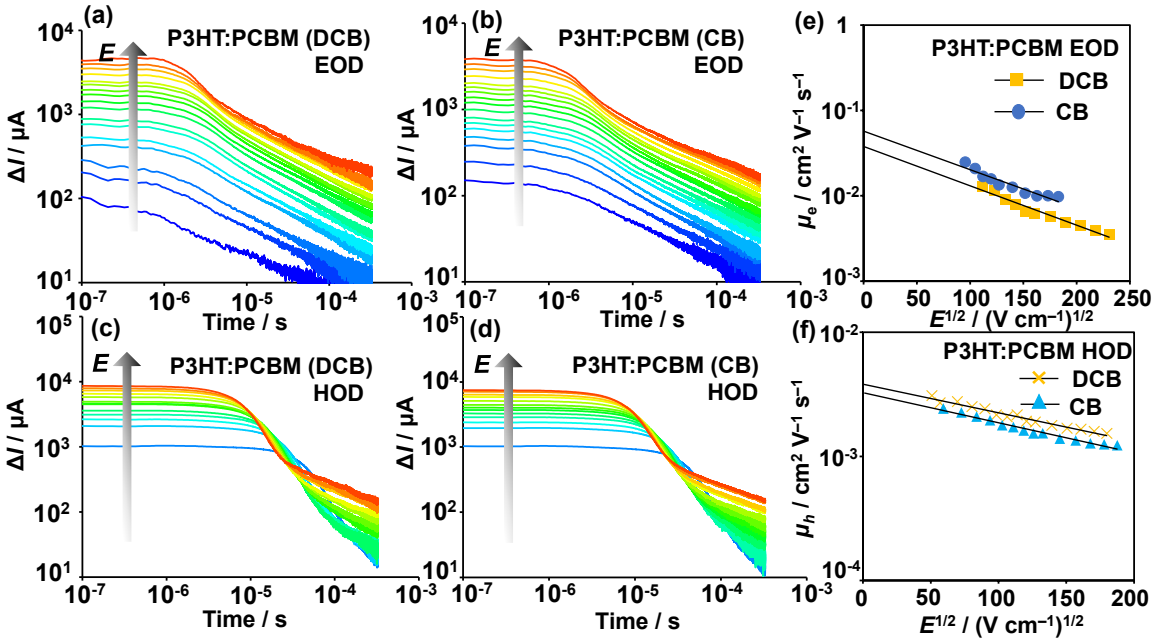

Figure S10. (a-d) Logarithmic plots of TPC decays for TOF measurements: (a-b) EOD of P3HT:PCBM (DCB) and P3HT:PCBM (CB) respectively. (c-d) HOD devices of EOD of P3HT:PCBM (DCB) and P3HT:PCBM (CB) respectively. The dark arrows show the increase of applied electric field strength from blue to orange lines: (a) (0.23–5.3) × 10^4 V cm^{-1}, (b) (0.15–3.3) × 10^4 V cm^{-1}, (c) (0.16–3.2) × 10^4 V cm^{-1}, (d) (0.18–3.5) × 10^4 V cm^{-1} (e-f): Plots of (e) electron and (f) hole mobility dependence on the square root of electric field strength *E*. The zero *E* mobility (μ_0) is derived by extrapolating to *E* = 0.

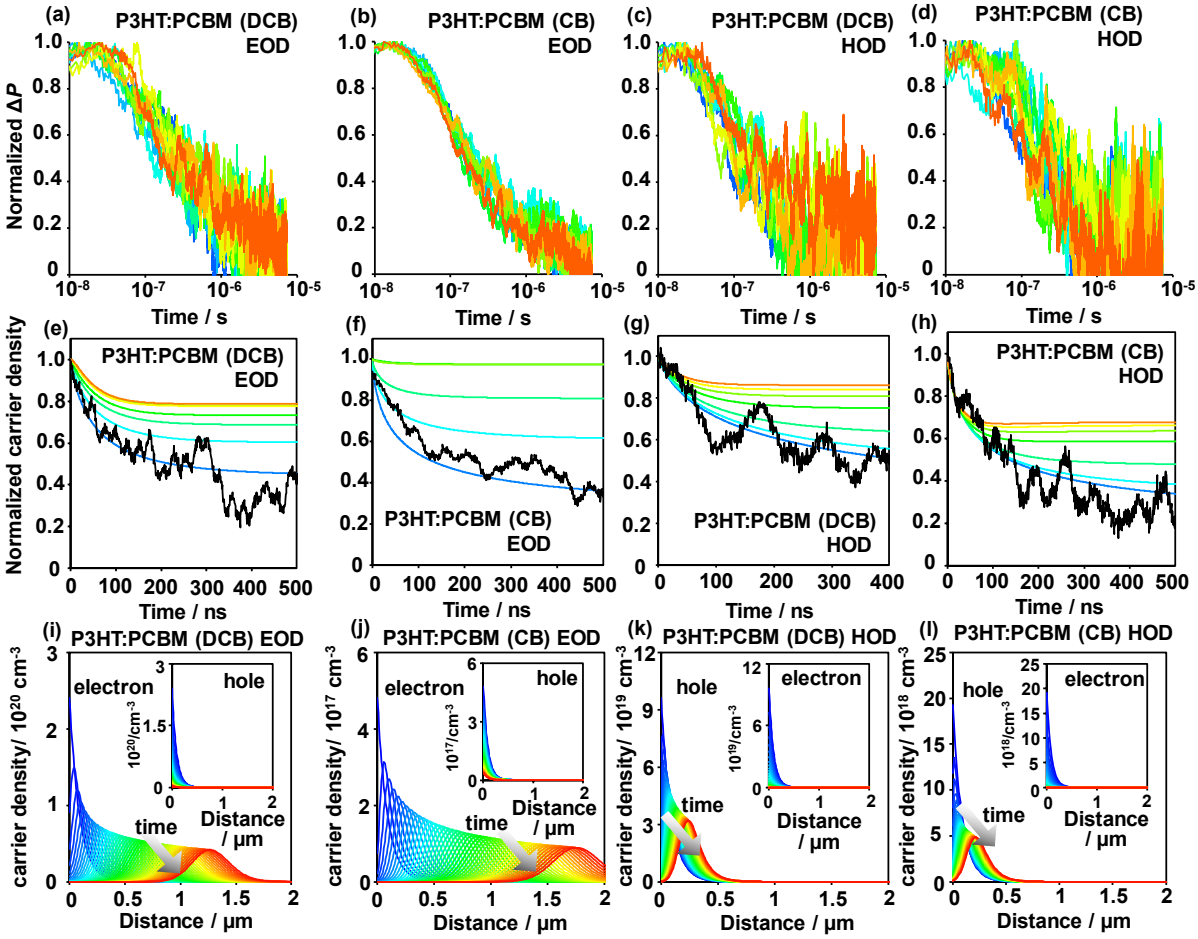

Figure S11. (a-d) Plots of the TRMC decays under the external *E*: (a) EOD of P3HT:PCBM (DCB), (b) EOD of P3HT:PCBM (CB), (c) HOD of P3HT:PCBM (DCB), (d) HOD of P3HT:PCBM (CB), respectively. Blue to oranges lines show the difference of applied electric field. (e-h): Normalized probability of EOD devices in (e) P3HT:PCBM (DCB) at *E*= (0.23–5.3) × 10^4 V cm^{-1} and (f) P3HT:PCBM (CB) at *E*= (0.22–3.3) × 10^4 V cm^{-1}, and of HOD devices in (g) P3HT:PCBM (DCB) at *E*= (0.26–3.2) × 10^4 V cm^{-1} and (h) P3HT:PCBM (CB) at *E*= (0.28–3.5) × 10^4 V cm^{-1}. (i-l): The time evolution of charge carrier spatial distribution (inset: the contrary charge carriers) of (i) P3HT:PCBM (DCB) EOD at *E*= 5.3×10^4 V cm^{-1}, (j) P3HT:PCBM (CB) EOD at *E*= 3.3×10^4 V cm^{-1}, (k) P3HT:PCBM (DCB) HOD at *E*= 3.2×10^4 V cm^{-1} and (l) P3HT:PCBM (CB) HOD at *E*= 3.5×10^4 V cm^{-1}.

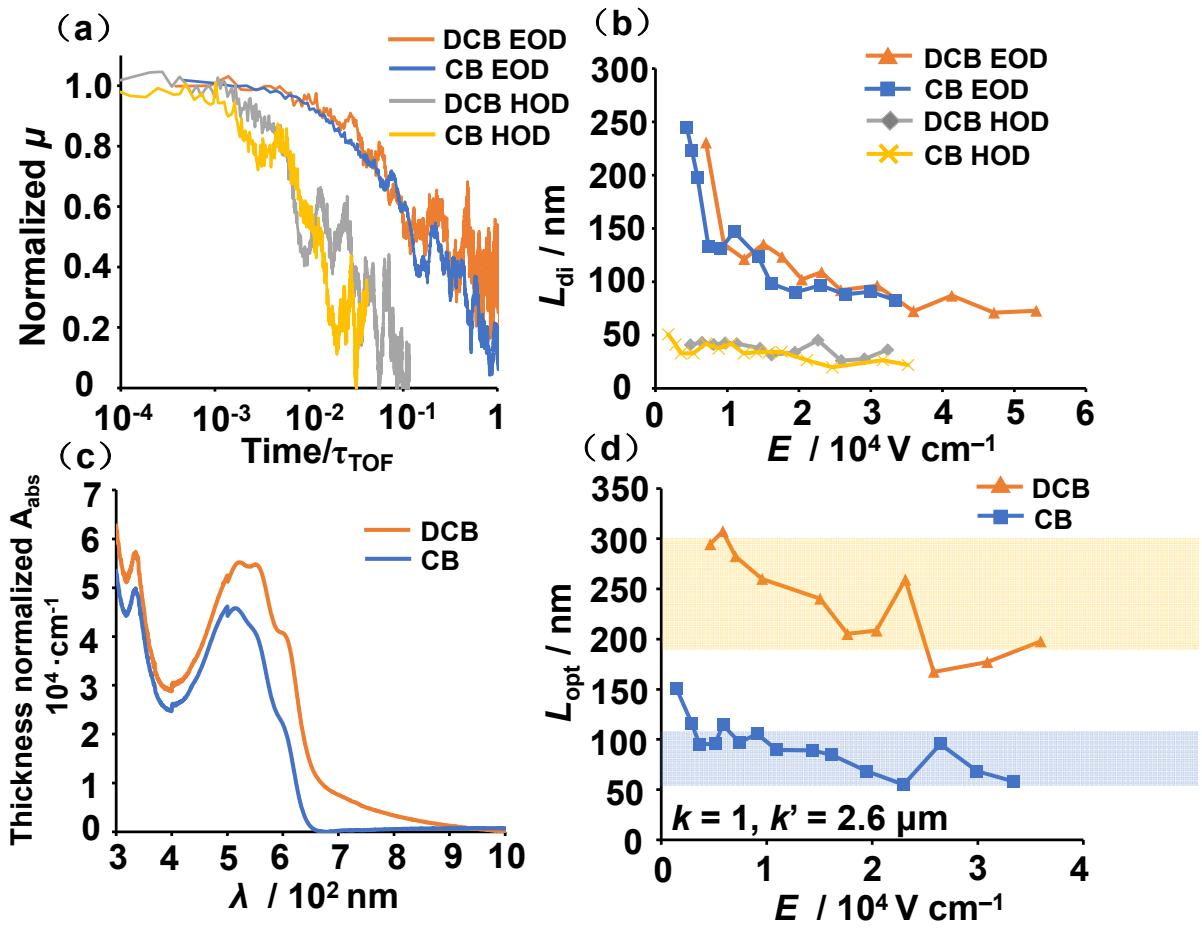

Figure S12. (a) Normalized mobility as a function of the normalized time (t/τ_{TOF}) (the profile of HOD at $t/\tau_{TOF} > 0.1$ is not shown, because of the large noise from baseline). The external electric field E for all of the selected profiles is approximately 2×10^4 V cm^{-1}. (b) Calculated diffusion length L_{di} as a function of external electric field strength. (c) Measured UV-vis absorption spectra of the BHJs. The absorption intensity is normalized by the thickness of samples. (d) The calculated L_{opt} as a function of external electric field strength. The coloured region shows the reported L_{opt} range in experiments.

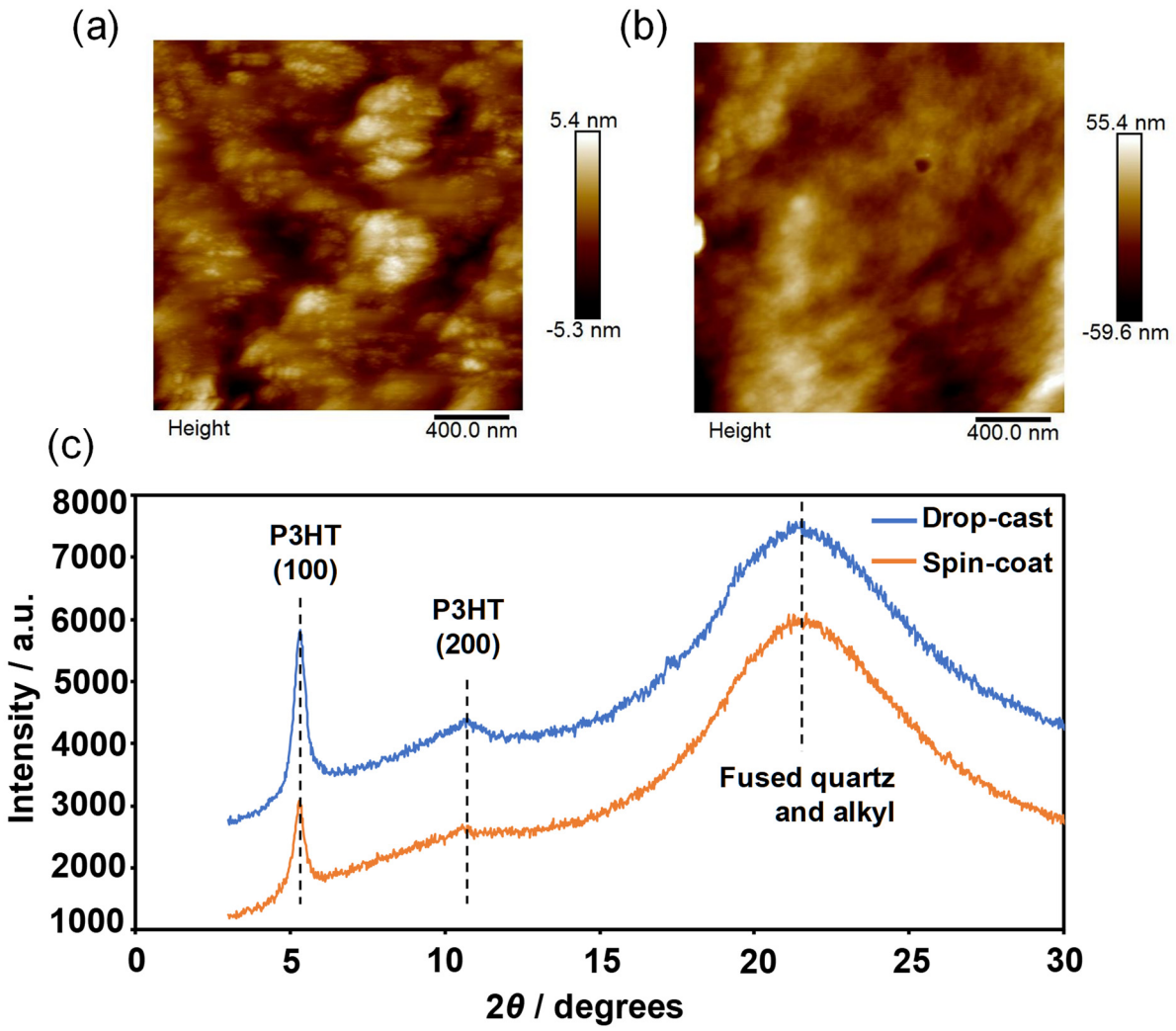

Figure S13. AFM images of P3HT:PCBM processed from DCB by (a) spin-coating (thickness ~ 95 ± 13 nm) and (b) drop-casting (thickness ~ 1035 ± 248 nm). (c) XRD diffraction patterns of the above P3HT-PCBM samples (substrate: fused quartz).

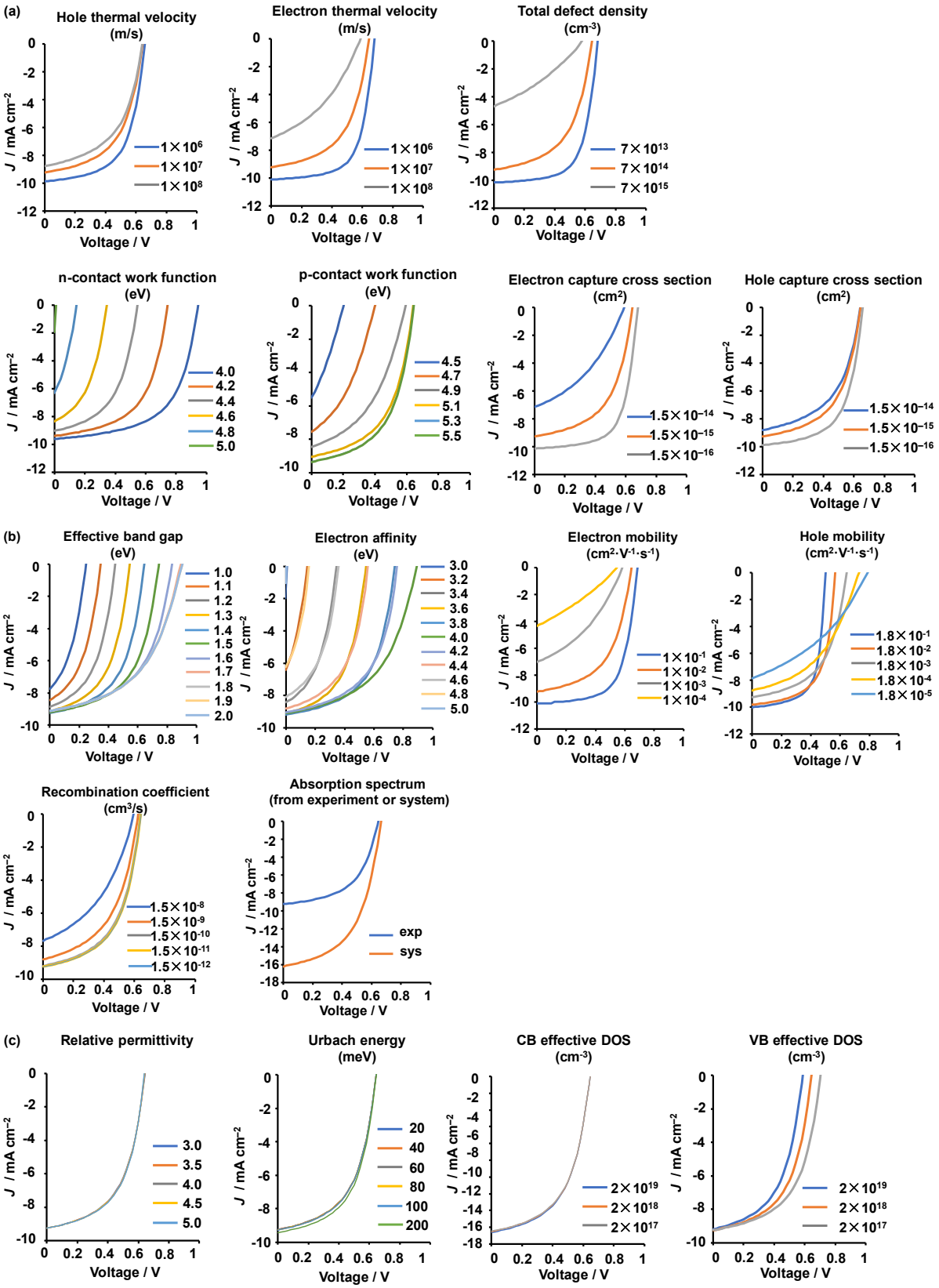

Figure S14. Sensitivity test of the SCAPS parameters. The sample is P3HT:PCBM with initial conditions shown in Table 2. The parameters are categorized into three group: a) important (a fitting parameter) (1st and 2nd rows), b) important (experimentally to be determined) (3rd and 4th rows), and c) not important (5th row). Each parameter is deliberately changed to see its effect on the resultant *JV* curve.